Proceedings of the XVII ECSMGE-2019
Geotechnical Engineering foundation of the future
ISBN 978-9935-9436-1-3

doi: 10.32075/17ECSMGE-2019-0958

XVII European Conference
ECSMGE 2019
Reykjavík
on Soil Mechanics
and Geotechnical Engineering

Breakage and critical state via DEM

Rupture et état critique via DEM

M. O. Ciantia
University of Dundee, School of Science and Engineering, Dundee, UK

C. O'Sullivan
Imperial College London, Dept. Civil and Environmental Engineering, London, UK

M. Arroyo, A. Gens
Universitat Politècnica de Catalunya, Dept. Civil and Environmental Engineering, Barcelona, Spain

ABSTRACT: Discrete-element simulations are used to explore the relation between breakage-induced grading evolution and the critical state line position on the compression plane. An efficient model of particle breakage is applied to perform a large number of tests, in which grading evolution is continuously tracked using a grading index. Using both previous and new experimental results, the discrete element model is calibrated and validated to represent Fontainebleau sand. The results obtained show that, when breakage is present, the inclusion of a grading index in the description of critical states is advantageous. This can be simply done using the critical state plane concept.

RÉSUMÉ: Les simulations d'éléments discrets sont utilisées pour explorer la relation entre l'évolution de la granulométrie induite par la rupture des grains et la position de la ligne d'état critique sur le plan de compression. Un modèle efficace de rupture des particules est appliqué pour effectuer un grand nombre de tests, dans lesquels l'évolution de la gradation est suivie en continu à l'aide d'un index de gradation. À l'aide des résultats expérimentaux précédents et nouveaux, le modèle d'éléments discrets est étalonné et validé pour représenter le sable de Fontainebleau. Les résultats obtenus montrent que la présence d'un indice de gradation dans la description des états critiques présente des avantages en cas de rupture. Ceci peut être fait simplement en utilisant le concept de plan d'état critique.

Keywords: Discrete-element modelling; particle crushing/crushability; sands; shear strength; stress path

1 INTRODUCTION

Sands shearing at constant volume and stress are in a critical state (CS). Different combinations of stress and volume are possible at the critical state: they form a critical state line (CSL). The state of sand during shearing processes would always move towards the CSL (Roscoe *et al*., 1958). Building upon these principles and using an elasto-plastic formalism the first constitutive models for sand were formulated (Roscoe et al., 1958). Many researchers have followed on that path (Gajo and Wood, 1999; Jefferies, 1993; Manzari and Dafalias, 1997; Russell and Khalili, 2004) producing more precise and realistic formulations of sand behaviour.

Quite frequently those models are formulated making use of a state parameter, a measure of the distance between a given state and the CSL. The most popular choice is the state parameter ψ first introduced by Wroth and Bassett (1965) and later

named as such by Been and Jefferies (1985). ψ is defined as the difference between current void ratio e, and e_c, void ratio on the critical state line at the same mean pressure. As this definition makes clear, the location of the CSL on the compression plane e-p' is quite important, as are the factors that may affect such location. In particular grading strongly affects the parameters defining the critical state line.

Materials such as carbonate sands (Bandini and Coop, 2011), volcanic pumice sands (Pender *et al.*, 2006) and rockfill (Xiao *et al*., 2016) show significant crushing at pressures well below 1 MPa. If quartz sands are tested at large stress (say above 5 MPa), grain crushing also becomes an important mechanism (Yamamuro and Lade, 1996). Cheng *et al*. (2004) used 400 DEM breakable agglomerates to explore the effect of breakage on CS and showed a lowering of the CSL. However, the void ratios were far above those typical of quartz sands and the limited number of grains represented resulted in noisy triaxial responses that made precise critical state identification difficult. A steeper CSL is not particularly problematic, what opens more questions is the idea that the CSL in the compression plane may become non-unique because of crushing. Muir Wood (2007) and Muir Wood & Maeda (2008) advanced the concept of a non-unique CSL. Conceiving grading as a further state variable they generalized the CSL into a plane, the critical state plane (CSP).

In this study DEM is used to obtain a more complete view of grading evolution and its relation to CS. A validated DEM model is applied systematically in triaxial conditions, with some 70 tests employed to explore the relations between grading evolution and critical states.

2 DEM MODEL DESCRIPTION

2.1 Particle failure criteria & calibration

To capture the rotational resistance that exists between non-spherical grains the rotation of the spherical DEM particles was inhibited (Ciantia *et al.*, 2014, 2016a, 2019). The contact model uses a simplified Hertz-Mindlin formulation and Coulomb friction. The limit criterion at which breakage is activated for a given particle was formulated following (Russell and Muir Wood, 2009). A particle breaks if the force F, at any of its contacts is such that

$$F = \sigma_{lim} \cdot A_F \tag{1}$$

where σ_{lim} is the limit strength of the material and A_F is the contact area. To incorporate the natural material variability into the model, the limit strength, σ_{lim}, is assumed to be normally distributed for a given sphere size. The coefficient of variation of the distribution, *var*, is taken to be a material parameter.

$$\sigma_{lim} = \sigma_{lim0} \cdot (d/d_0)^{-3/m} \tag{2}$$

Once the limit condition is reached, a particle, will split into 14 smaller inscribed tangent spheres. Using a simplified Hertz-Mindlin to describe the contact area eq. (1) results

$$F \leq \left\{ \sigma_{lim} \left(\frac{d}{d_0}\right)^{\frac{-3}{m}} \pi \left[\frac{3}{4} \frac{\left(\frac{1-\nu_1^2}{E_1}+\frac{1-\nu_2^2}{E_2}\right)}{\left(\frac{1}{r_1}+\frac{1}{r_2}\right)} \right]^{\frac{2}{3}} \right\}^3 \tag{3}$$

where r_1 and r_2 are the radii of the contacting spheres and E_i, ν_i are the Young's Moduli and Poisson's ratio respectively. Note that this breakage criterion does not involve exclusively the maximum force on the particle: there is a strong inbuilt dependency on the characteristics of the contacting particles Full details of the model are reported in Ciantia et al. (2015). To create a sample that is a representative volumetric element (REV) a cubic volume is filled with particles using the radius expansion method. Specimen boundaries are defined using smooth "wall" elements, so that the principal axes of stress and strain are coincident with the cube axes. Gravity

is set to zero and a servo-controlled motion of the cube walls applies pre-defined stress-paths. The PFC3D code (Itasca, 2017) is used for all simulations. Particle sizes for the numerical cubical cell are selected to closely match the grain size distribution of Fontainebleau NE34 sand (Figure 1b), with particle diameters ranging from 0.1 to 0.4 mm. Results from a previous study (Ciantia et al., 2016b) indicate that, for this sand, a cube with side lengths of 4 mm containing 10,000 particles is large enough to obtain smooth numerical responses and can be considered as a representative element volume (REV). The calibrated model parameters are collected in Table 1.

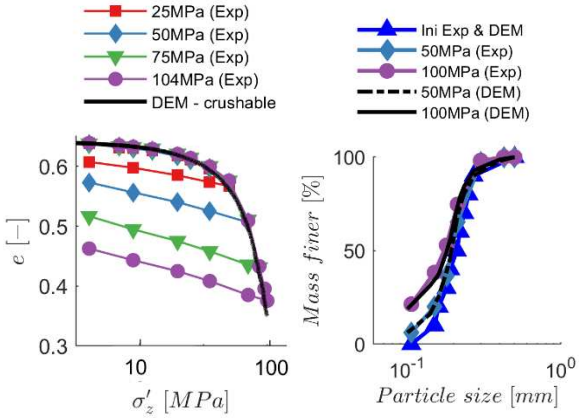

Figure 1. DEM and experimental curves of a) oedometric compression test and b) PSD evolution.

The elasto-plastic contact law parameters (G, υ, μ) were calibrated by simulating a couple of drained triaxial tests on dense and loose specimens at low confining pressure (100 kPa) reported by Seif El Dine et al., (2010). The within size particle strength variability parameter (*var*) was obtained fitting a Gaussian distribution curve to single grain crushing experiments on another silica sand. The parameter controlling grain size effect on strength, *m*, was obtained considering experimental data on flat platen single particle crushing forces on different silica sands. σ_{lim0} was selected to capture the apparent yield point of an oedometer (Figure1a).

Table 1. DEM input parameters for simulation

d_{50} mm	μ -	G GPa	ν -	$\sigma_{lim,0}$ GPa	m -	d_0 mm	var -
0.21	0.27	3	0.3	5	10	2	1

3 CRITICAL STATES AND GRADING

To inspect the effect of grading evolution on critical state (CS) triaxial tests simulations were performed on the Fontainebleau sand discrete analogue. The initial void ratio for all tests was 0.65 which is equivalent to a relative density of 65% for NE34 FS. Five series of tests were used for this purpose. In the first series (A) the crushable model was isotropically loaded up to confining pressures of 0.5, 6, 16 and 30 MPa and then sheared at constant confining pressure σ_c, at constant mean stress, p' and at constant vertical stress σ_v. In the second series (B) the same tests were performed, bu the crushing module was disabled before testing. In the third series (C) the crushable model was active during isotropic loading up to 60 MPa. At that stage crushing was disabled and the model was unloaded to 0.5, 6, 16 and 30 MPa isotropic stress (i.e. OCR = 120, 10, 3.75 and 2). From each of this overconsolidated states three triaxial tests were performed (again with either σ_c, p' or σ_v constant). The fourth series (D) was like the third, but now isotropic preloading took place up to 100MPa. The fifth series (E) was another variant of the third, in which the crushing model was always enabled and including only unloading to 6 and 30 MPa (i.e. OCR = 10 and 2). All tests continued up to deviatoric strains of 30%. At that strain level conventionally defined critical state conditions (i.e. a constant level of mobilized shear strength and void ratio) were clearly identifiable from the simulations. In this work, the grading index I_G, is computed as the area ratio of the current grading to a limit grading. Refer to Ciantia *et al*. (2019) for more details.

3.1 Grading evolution effect on CS

Figure 2 presents the stress paths for all tests in series A and B, with indication of the peak and

critical state strengths identified on each path. For the crushable material the difference between peak and critical strength disappears at high pressures.

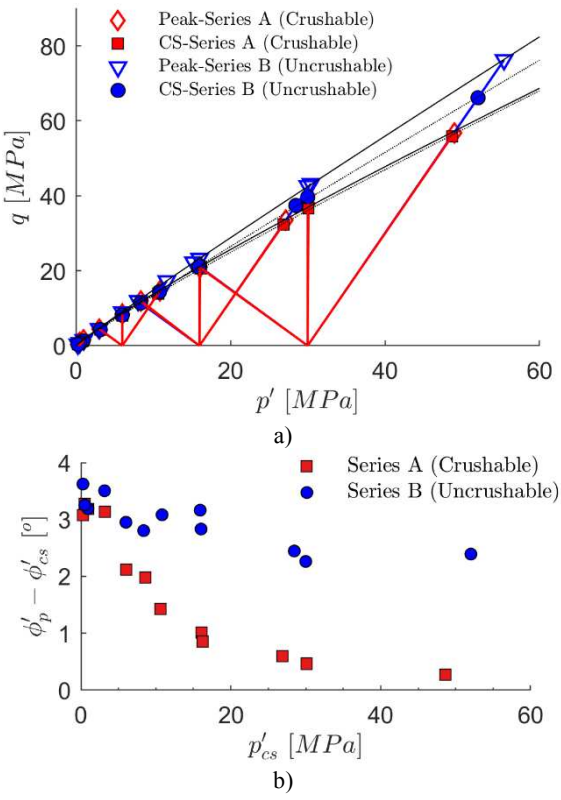

Figure 2. Test series A (crushable material; OCR = 1) and B (uncrushable material; OCR = 1) (a) peak and critical state envelopes (b) mobilised friction angle vs mean stress at peak and critical state.

The isotropic compression and shearing paths from test series A & B are presented in e-log p' space in Figure 3a. The end points of the shearing paths are used to delineate a tentative CSL for both crushable and uncrushable materials. For the uncrushable case ICL and CSL seem to converge at large pressures. For the crushable case, the two lines appear to cross each other and later become parallel, a feature also observed in experiments in crushable sands (Bandini and Coop, 2011). For the uncrushable case the CSL remains above the ICL and all tests dilate to arrive to critical conditions, for the crushable case the material dilates at low pressure and contracts at high pressure to reach critical conditions.

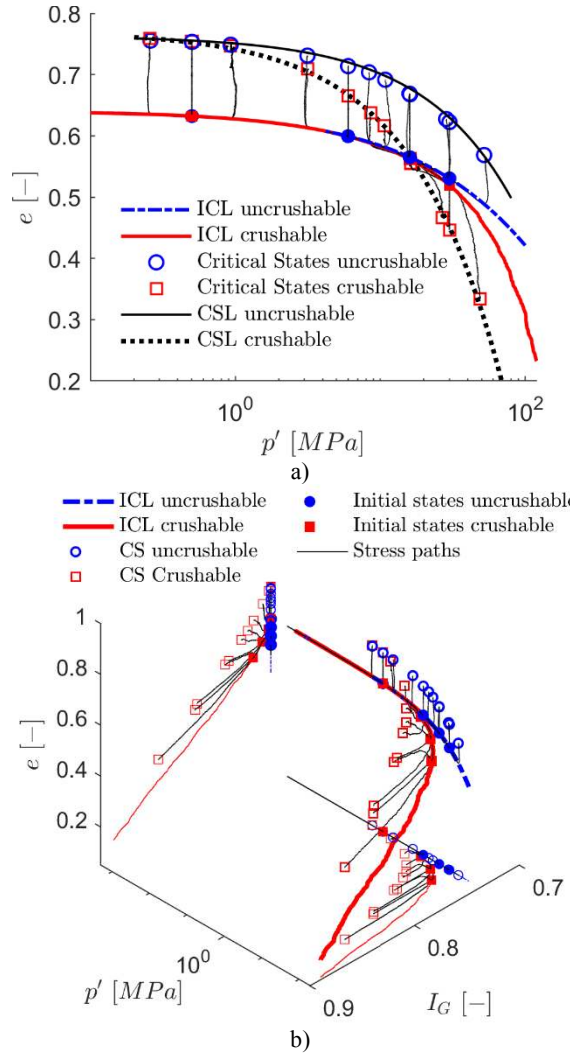

Figure 3. Crushable and Uncrushable Critical state investigation: a) state evolution in p'-e plane and b) state evolution in e-p'-I_G space with corresponding 2D projections.

We can add here a third dimension to the graph: the grading index. Figure 3b presents a three-dimensional view of the ICL and shearing paths towards critical state. In this enriched space, it appears that the CSL for the crushable

soil does not actually cross the ICL, but rather rotates or curls around it. Two new projections of the results are also possible. The first represents the ICL on the log p' vs I_G plane and shearing paths towards the CSL. The faster grading evolution induced by shearing is clear in this plane, as well as the fact that this only happens for shearing paths starting after the isotropic yield –i.e. starting after I_G has already increased on the isotropic path. The second projection uses an e vs I_G plane. It shows that, for this initially dense sand, while dilation during shear is still taking place, grading evolution is relatively moderate, whereas overall contraction during shear is indicative of a very active crushing process.

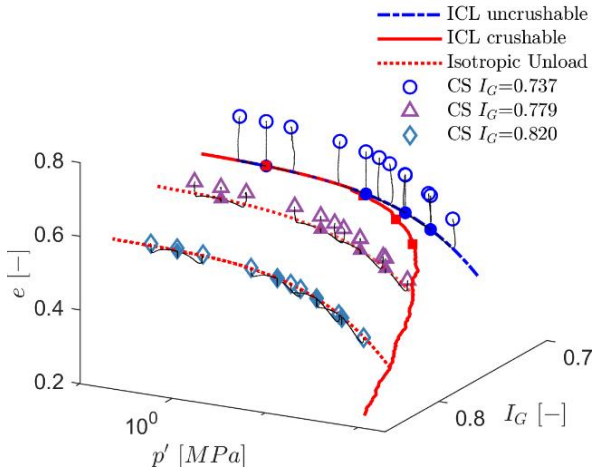

Figure 4. State evolution in e-p'-I_G space including two unload paths and stress paths of other 24 shear tests to critical state where crushing is inhibited.

3.2 CS at fixed grading

The three-dimensional view just introduced is employed also in Figure 4, to present the results of test series B, C & D, in which crushing is disabled during shear. Shearing here proceeds at constant I_G. It is clear that the critical states of series B (I_G = 0.737) align themselves well above those of test series C (I_G = 0.779), which themselves lie above those of test series D (I_G = 0.820). In Figure 5 three CSL are fitted to the critical state points attained at constant grading using the following expression

$$e_c = \Gamma + \gamma \left(\frac{p'}{p_a}\right)^{0.7}. \quad (4)$$

Normalization of the isotropic stress axis follows here the suggestion of Li and Wang (1998). A very good fit is obtained with the shifted curves having practically identical slopes. Still, the slope at the wider grading (I_G = 0.82) is 6% higher than that at the initial grading. Similar observations are reported by Muir Wood & Maeda (2008). These curves at constant grading will be subsequently referred to as $CSL_{IG=x}$, with the x in the subscript being a placeholder for the relevant I_G value.

The extent of the parallelism between the CSLs obtained with different gradings is such that a single plane can be fitted in the three-dimensional space that includes the grading index, Figure 6. The equation of this critical state plane (CSP) is

$$e_c = \alpha + \beta I_G + \delta \left(\frac{p'}{p_a}\right)^{0.7} \quad (5)$$

with a best fit for FS given by α=2.553, β=-2.441 and δ=-0.002325 (R^2>0.99) and α=6.435, β=-5.882 and δ=-0.04845 (R^2>0.87) for Dogs Bay sand (see Ciantia et al., 2019).

3.3 CS with evolving grading

The critical state points established for the normally consolidated crushable material (i.e. in test series A), can also be used to fit a CSL using eq. (4) and are represented in Figure 5. This CSL at variable grading, which we will denote CSL_{nc}, has a much steeper gradient than the $CSL_{IG=0.737}$, $CSL_{IG=0.779}$, $CSL_{IG=0.82}$ obtained at fixed gradings. This CSL_{nc} is, of course, the same as the CSL classically identified in previous studies of crushable sands (e.g. Coop and Lee, 1993).

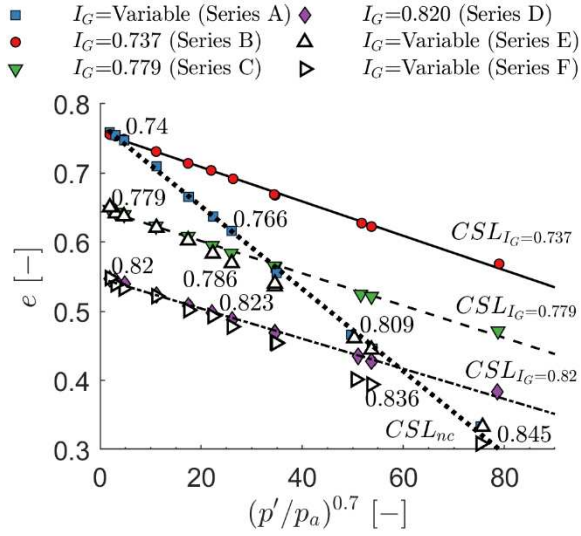

Figure 5. CSL for fixed and variable grading and critical state points obtained for all test series.

The CSL_{nc} identified in test with variable grading belongs into the same critical state plane previously identified by testing at fixed gradings. Figure 6 shows that the CSP equation - obtained with data at constant grading - predicts very well the critical state points at variable grading.

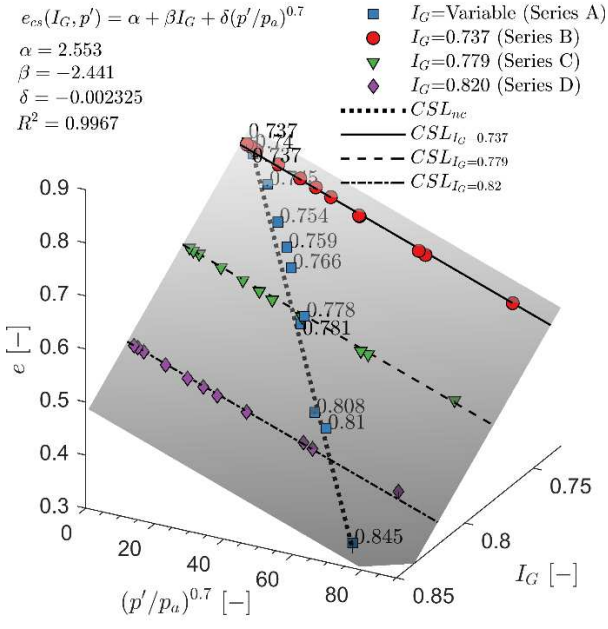

Figure 6. Definition of CSP as a function of Ig-e-p'.

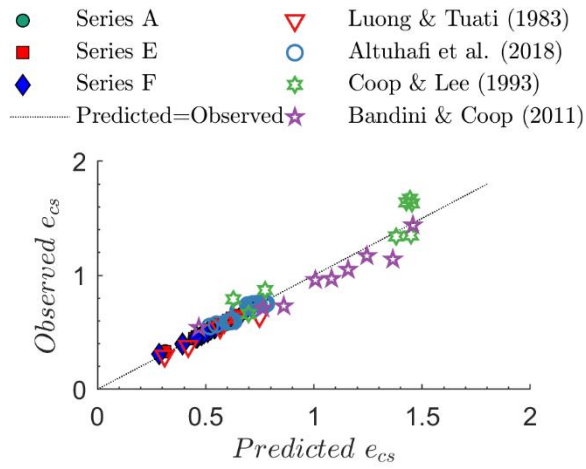

Figure 7. Critical state values for evolving grading: predicted values from the CSP plotted against observed values.

Of course, this has a significant practical implication: the experimental data used to obtain a CSL_{nc} may also be used to fit a CSP if care is taken (a) to supplement each critical state data point with information about final grading (b) to collect enough data points to fit three parameters instead of two. Figure 7 also reports experimentally obtained critical state data for Fontainebleau sand (Altuhafi et al., 2018) and Dogs Bay sand (Bandini and Coop, 2011; Coop and Lee, 1993) reinterpreted using the CSP concept (see Ciantia et al., (2019) for the CSP fitting parameters of Dogs Bay sand).

Are then the CSL_{nc} and CSP fully equivalent? An answer may be found by examining the results of tests performed on a crushable material at overconsolidated states, i.e. the results of test series E. Figure 5 also represents the critical state points obtained from these tests together with the different CSL previously defined. It is apparent that for series E, only those tests attaining critical state at the highest pressures plot on top of the CSL_{nc}. On the other hand, all tests, without exception, attain a critical state at points very close to the CSP (Figure 6). It seems then that the predictive power of the CSP extends farther than that of the CSL_{nc}. Examining those tests attaining CS at the lowest pressure (those with the highest

OCR) appear very close to a CSL obtained at constant grading, namely $CSL_{IG=0.779}$. That line was obtained at the I_G value (I_G = 0.779) that specimens in test series E had just before unloading. Why would this value be only relevant to the more highly overconsolidated specimens? The answer requires a more general consideration of the grading evolution pattern.

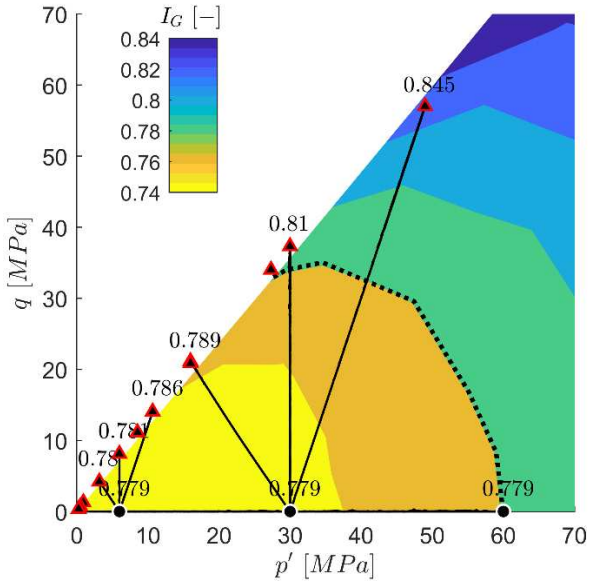

Figure 8. Stress paths of OC samples (test series E) superimposed on the iso-I_G map.

Ciantia *et al*. (2019) show how grading evolves in the triaxial plane during radial compression tests i.e. during tests at constant η = q/p' taken up to p' = 120 MPa. The data obtained from these tests is re-elaborated in Figure 8 to obtain *iso-I_G* maps on the triaxial plane p'-q. The shapes of these curves recall the theoretical yield curves for the crushing mechanism postulated by Kikumoto et al. (2010). Superimposing the shearing stress paths from test series E on a map in which the I_G = 0.779 isocurve has been highlighted. It appears that the stress paths starting at OCR = 10 do not cross that curve until practically at the shear critical state. On the other hand, the OCR = 2 paths do cross the curve well before the shear critical state is attained. The response observed seems compatible with the activation of an independent crushing plastic mechanism.

4 CONCLUSIONS

The results obtained support unequivocally the hypothesis of a multiplicity of critical state lines for crushable materials. However that multiplicity does not imply any ambiguity since, at any moment in time only one grading is effective and that grading has a unique $CSL_{IG=x}$ associated. All the $CSL_{IG=x}$ belong into a unique critical state plane. That critical state plane also includes the classically identified CSL_{nc}, which actually only strictly pertains to the normally consolidated material. At low values of OCR, though, the difference between observed critical states and those attained from the CSL_{nc} would be small, since the shearing path towards critical state would involve renewed crushing. At high values of OCR the material would attain the critical states that are linked to the grading attained during previous compression.

The CSP expression, derived for a strong silica sand, is a very powerful tool capable to predict the CS void ratio also for other more crushable sands. For instance, Figure 5 shows how the calibrated CSP proposed by Ciantia *et al*. (2019), predicts quite well also the critical state void ratio of Dogs Bay sand.

Grading evolution may be present in some geotechnical applications, particularly those involving some kind of intense preloading of a crushable material. A systematic consideration of grading evolution and its consequences would be helpful in extending critical state soil mechanics principles to those cases.

5 ACKNOWLEDGEMENTS

The BGA and the ISSMGE are gratefully acknowledged for having covered part of the travel and conference fees of the first author.

6 REFERENCES

Altuhafi, F.N., Jardine, R.J., Georgiannou, V.N., Moinet, W.W., Ciantia, M.O., Arroyo, M., Gens, A., 2018. Effects of particle breakage and stress reversal on the behaviour of sand around displacement piles. *Géotechnique* 1–2.

Bandini, V., Coop, M.R., 2011. The influence of particle breakage on the location of the critical state line of sands. *Soils Found*. **51**, 591–600

Been, K., Jefferies, M.G., 1985. A state parameter for sands. *Géotechnique* **35**, 99–112.

Cheng, Y.P., Bolton, M.D., Nakata, Y., 2004. Crushing and plastic deformation of soils simulated using DEM. *Géotechnique* **54**, 131–141

Ciantia, M.O., Arroyo, M., Butlanska, J., Gens, A., 2014. DEM modelling of a double porosity crushable granular material. Proc. Int. Symp. Geomech. from Micro to Macro 269–274

Ciantia, M., Arroyo, M., O'Sullivan, C., Gens, A., Liu, T., 2018. Grading evolution and critical state in a discrete numerical model of Fontainebleau sand. *Géotechnique*. **69**, 1-15

Ciantia, M.O., Arroyo, M., Calvetti, F., Gens, A., 2015. An approach to enhance efficiency of DEM modelling of soils with crushable grains. *Géotechnique* **65**, 91–110.

Ciantia, M.O., Arroyo, M., Butlanska, J., Gens, A., 2016a. DEM modelling of cone penetration tests in a double-porosity crushable granular material. *Comput. Geotech.* **73**, 109–127.

Ciantia, M.O., Arroyo, M., Calvetti, F., Gens, A., 2016b. A numerical investigation of the incremental behavior of crushable granular soils. *Int. J. Numer. Anal. Methods Geomech.* **40**, 1773–1798.

Coop, M.R., Lee, I.K., 1993. The behaviour of granular soils at elevated stresses. In: Houlsby, G.T., Wroth, P., Schofield, A.N. (Eds.), Predictive Soil Mechanics. Thomas Telford Ltd, pp. 186–198.

Gajo, A., Wood, M., 1999. Severn–Trent sand: a kinematic-hardening constitutive model: the q–p formulation. Géotechnique 49, 595–614.

Itasca, C.G.I. 2017. *Particle Flow Code*, Ver. 5.0.

Jefferies, M.G., 1993. Nor-Sand: a simle critical state model for sand. *Géotechnique* **43**, 91–103.

Kikumoto, M., Wood, D.M., Russell, A., 2010. Particle Crushing and Deformation Behaviour. *Soils Found*. **50**, 547–563.

Li, X.S., Wang, Y., 1998. Linear Representation of Steady-State Line for Sand. *J. Geotech. Geoenvironmental Eng.* **124**, 1215–1217.

Manzari, M.T., Dafalias, Y.F., 1997. A critical state two-surface plasticity model for sands. *Géotechnique* **47**, 255–272.

Muir Wood, D., 2007. The magic of sands - The 20th Bjerrum Lecture presented in Oslo, 25 November 2005. *Can. Geotech. J.* **44**, 1329-50

Pender, M.J., Wesley, L.D., Larkin, T.J., Satyawan, P., 2006. Geotechnical properties of a pumice sand. *Soils Found.* **46**, 69–81.

Roscoe, K.H., Schofield, A.N., Wroth, C.P., 1958. On The Yielding of Soils. *Géotechnique* **8**, 22–53.

Russell, A.R., Khalili, N., 2004. A bounding surface plasticity model for sands exhibiting particle crushing. *Can. Geotech. J.* **41**, 1179–1192.

Russell, A.R., Muir Wood, D., 2009. Point load tests and strength measurements for brittle spheres. *Int. J. Rock Mech. Min. Sci*. **46**, 272–280.

Seif El Dine, B., Dupla, J.C., Frank, R., Canou, J., Kazan, Y., 2010. Mechanical characterization of matrix coarse-grained soils with a large-sized triaxial device. *Can. Geotech. J.* **47**, 425–438.

Wood, D.M., Maeda, K., 2008. Changing grading of soil: Effect on critical states. *Acta Geotech*. **3**, 3–14.

Wroth, C.P., Bassett, R.H., 1965. A Stress–Strain Relationship for the Shearing Behaviour of a Sand. *Géotechnique* **15**, 32–56.

Xiao, Y., Liu, H., Ding, X., Chen, Y., Jiang, J., Wengang Zhang, 2016. Influence of Particle Breakage on Critical State Line of Rockfill Material. *Int. J. Geomech*. **16**, 04015031.

Yamamuro, J.A., Lade, P. V., 1996. Drained Sand Behavior in Axisymmetric Tests at High Pressures. *J. Geotech. Eng.* **122**, 109–119.